RSC Advances

PAPER

View Article Online
View Journal | View Issue

Open Access Article. Published on 06 March 2017. Downloaded on 10/23/2025 5:22:54 PM.
This article is licensed under a Creative Commons Attribution 3.0 Unported Licence.

Cite this: *RSC Adv.*, 2017, 7, 14649

A glassy carbon electrode modified with γ-Ce_2S_3-decorated CNT nanocomposites for uric acid sensor development: a real sample analysis†

Mohammed M. Rahman,*[ab] Jahir Ahmed[c] and Abdullah M. Asiri[ab]

γ-Ce_2S_3-decorated multi-walled carbon nanotube nanocomposite (Ce_2S_3-CNT NC) was synthesized by a wet chemical method in basic phase. Characterization of the resulting Ce_2S_3-CNT NCs was performed in detail by field emission scanning electron microscopy (FE-SEM) attached with energy dispersive spectroscopy (EDS), X-ray photoelectron spectroscopy (XPS), UV/vis spectroscopy, FT-IR spectroscopy, and X-ray diffraction (XRD). A glassy carbon electrode (GCE) was fabricated using the Ce_2S_3-CNT NCs and then it was utilized to develop a biological sensor for the detection of uric acid (UA) *via* a simple electrochemical approach. With the selectivity study, UA was selected as a target since it exhibited a fast response towards the Ce_2S_3-CNT NC-fabricated GCE sensor in the *I*–*V* method. The fabricated sensor also displayed an excellent sensitivity, very low detection limit, long-term stability, and reproducibility. In the diagnostic study, a linear calibration plot ($r^2 = 0.9972$) was obtained for 0.1 nM to 1.0 mM aqueous UA solution, with the sensitivity value of 1.5822 μA nM^{-1} m^{-2} and an extremely low detection limit LOD = 60.0 ± 0.05 pM (S/N = 3). Potentials of the Ce_2S_3-CNT NCs in terms of biological sensing were also investigated *via* real serum and urine sample analyses. This approach is emerging as an effective technique in the development of an efficient biological sensor for the detection of biochemicals in broad scales.

Received 27th November 2016
Accepted 21st February 2017

DOI: 10.1039/c6ra27414e

rsc.li/rsc-advances

1. Introduction

Uric acid (UA) is an important biomolecule that is often present in blood serum, urine, or biological fluids and is excreted from the human body.[1,2] UA is a product of the metabolite of purine nucleotides, nucleic acids, and nucleoproteins.[3] Due to its poor solubility in water (approximately 60 mg L^{-1}), UA can easily accumulate in human body. Moreover, UA when present in excess in the body fluid can also solidify as a urate, which may cause gout or kidney stones.[4] High uric acid concentration in the blood may lead to deterioration of the renal function and also causes several diseases such as gout, myocardial infarction, hyperuricemia, physiological disorders, and Lesch–Nyhan syndrome.[5–7] Therefore, monitoring the uric acid level in the body fluid is sometimes considered as a key factor for the evaluation of a health condition.[8] Therefore, detection of UA is essential for diagnosis as well as public health monitoring. Various enzyme-based sensors have already been reported for UA detection. However, enzymes can properly work only under appropriate conditions and hence these sensors cannot be used for a wide range of applications. On the other hand, non-enzymatic biosensors are more versatile.[2] Electrochemical sensors always offer fast, profound, and cost-effective methods in UA detection and quantification.[9,10] However, the electrochemical response of UA at a bare electrode is kinetically slow and often associated with high overpotential. Consequently, searching for new materials for the modification of electrodes to enhance the rate of electron transfer and reduce the overpotential is required.[11] Carbonaceous materials such as CNT, graphene oxides, carbon black, fullerenes, *etc.* exhibit promising electrocatalytic properties.[12–15] Liu *et al.* proposed a CNT composite-based sensor for electrically conductive strain sensing, conductive thermoplastic polyurethane–graphene nanocomposite-based organic vapor sensing, and a strain sensor based on conductive thermoplastic elastomer-graphene nanocomposites.[16–18]

Several redox mediators such as pristine graphene,[1] gold nanocluster,[3] Au–Pt bimetallic nanoclusters decorated on graphene oxide,[19] mesoporous nickel oxide,[3] polypyrrole films doped with ferrocyanide ions onto an iron substrate,[20] reduced graphene oxide/zinc sulfide nanocomposite,[21] calixarene-modified glassy carbon electrode,[22] flexible graphene fibers,[23] poly(glyoxal-bis(2-hydroxyanil))-fabricated GCE,[24] CeO_2 nanoparticle-fabricated glassy carbon paste electrode,[25] iron nanoparticle-fabricated MWCNT enriched carbon paste electrode,[26] carbon nanohorns/poly(glycine)-modified glassy carbon electrode[27] *etc.* have been developed to date for the modification of the electrode in UA

[a]*Center of Excellence for Advanced Materials Research (CEAMR), King Abdulaziz University, P.O. Box 80203, Jeddah 21589, Saudi Arabia. E-mail: mmrahman@kau.edu.sa; mmrahmanh@gmail.com; Fax: +966-12-695-2292; Tel: +966-59-642-1830*

[b]*Chemistry Department, Faculty of Science, King Abdulaziz University, P.O. Box 80203, Jeddah 21589, Saudi Arabia*

[c]*Department of Chemistry, School of Physical Sciences, Shahjalal University of Science and Technology, Sylhet-3100, Bangladesh*

† Electronic supplementary information (ESI) available. See DOI: 10.1039/c6ra27414e

Open Access Article. Published on 06 March 2017. Downloaded on 10/23/2025 5:22:54 PM.
This article is licensed under a Creative Commons Attribution 3.0 Unported Licence.

detection; however, all these attempts are either time consuming, require sophisticated instruments or are not cost-effective for routine analysis. Moreover, due to low-cost, rapid response, and higher sensitivity, electrochemical sensors are often considered more useful than any other methods for UA detection. For the real IT application of sensors, the challenge is due to advances in device fabrication, mechatronics, and communication technologies and limited availability of sophisticated sensor and actuator devices. It targets both everyday life industrial and mission-critical needs, which are either confined to a single target device or distributed within a network of units, by also taking advantage of seamless communication capabilities and address different application scenarios.[28] These represent mostly relate to ecology or environment in which they are placed through active sensors and actuators, hence setting the IT technological bases for the cyber-physical framework. In some cases, sensors and actuators can be cybernetic or virtual when physical entity is not there but data-streams are generated and decisions are appropriately taken based on the information provided. For an environmentally intelligent sensor, table-top object manipulation is one of the most collective tasks, which combines the capabilities of robotic vision, image processing, object recognition, hand-arm manipulation, *etc.* However, the real indoor environment is much more convoluted than experimental scenarios. Sometimes the vision of a robot can hardly offer enough information for successfully executing some challenging tasks such as picking, placing or assembling some small targeting objects. In these circumstances, if two objects are too close to each other, it is difficult to correctly segment them; moreover, some occlusion cases often occur in the real indoor environment. Thus, a tele-operative demonstration method is an efficient way to overcome these problems. These demonstration techniques have already been implemented on industrial robots for several years.[29]

Recently, nanostructured transition metal sulfides have become more important in the research field due to their excellent electrochemical properties.[30] Cerium sulfides show important roles as electrocatalysts among all other transition metal sulfides. To date, core–shell structured Ce_2S_3 on ZnO, Ce_2S_3 on SiO_2, undoped and sodium-doped γ-Ce_2S_3 amorphous cerium sulphides, cerium sulfide/graphene nanocomposites, *etc.* have been prepared;[31,32] however, these efforts have become unsuccessful in improving the electrochemical properties of cerium sulfides because of ineffective external interaction between cerium sulfides and carbonaceous substances. This ineffective communication among redox active entities and charge-transfer materials will only allow the fractional cerium sulfide molecules to join in the electron transfer process. Hence, unexpected electrochemical properties of cerium sulfides achieved slower charge-transfer than that of carbonaceous materials. To overcome these complications, herein, we proposed a facile wet-chemical method to prepare Ce_2S_3-CNT NCs in the form of interconnected three dimensional conductive links where Ce_2S_3 nanostructures are attached in and around CNT. Dispersed CNT solution plays a role as a precursor in these attachments, where γ-Ce_2S_3 nanoparticles are deposited in and around the CNT. An important benefit of these nanocomposites is that nanostructured cerium sulphides are firmly attached to the CNT and these two different entities are rigidly joined together. The as-grown nanocomposite Ce_2S_3-CNT NC exhibits unprecedented electrochemical performance. Since the improvement of the electrochemical properties of CNT, by making them nanocomposites, is cost-effective and quick relative to that of others reported in the literature,[24] herein, we proposed an electrochemical sensor for the detection and quantification of UA in aqueous solutions (even at pico molar level) using Ce_2S_3-CNT NC-fabricated GCE. To the best of our knowledge, a Ce_2S_3-CNT NC-fabricated GCE sensor has not been reported to date, and herein, this sensor displays the lowest detection limit (LOD = 60.0 ± 0.05 pM) for the detection of UA than any other reported sensor.

2. Experimental

2.1. Materials and methods

Cerium(III)chloride heptahydrate ($CeCl_3 \cdot 7H_2O$), hydrated sodium sulphide ($Na_2S \cdot 9H_2O$), ethanol, disodium phosphate, monosodium phosphate, multi-walled CNT, creatinine, cystine, glycine, leucine, thionin acetate, tyrosine, uric acid, Nafion (5% ethanolic solution), and acetone were used without any further purification and were purchased from the Sigma-Aldrich Company. Ce_2S_3-CNT NCs was investigated *via* UV/vis spectroscopy (Evolution 300 UV/visible spectrophotometer, Thermo scientific). An FT-IR spectrum was obtained for the Ce_2S_3-CNT NCs using a spectrophotometer (NICOLET iS50 FTIR spectrometer, Thermo scientific.) in the range from 400 to 4000 cm^{-1}. The XPS measurements were carried out to estimate the binding energies in eV for C, Ce, and S using a Mg$K\alpha_1$ spectrometer (Thermo scientific, Kα 1066, USA) with an excitation radiation source (Al Kα, beam spot size = 300.0 μm, pass energy = 200.0 eV, and pressure $\sim 10^{-8}$ torr). The powdered XRD spectrum was obtained by an X-ray diffractometer (XRD, Thermo scientific, ARL X'TRA diffractometer) with Cu $K\alpha_1$ radiation ($\lambda = 1.5406$ nm) using the generator voltage of 40 kV and current of 35 mA applied for the measurement. Morphologies of the Ce_2S_3-CNT NCs were investigated by FESEM (JEOL, JSM-7600F, Japan). Elemental analysis was carried out by EDS (JEOL, Japan). *I–V* measurements were performed by the Keithley, 6517A Electrometer, USA, at 25.0 °C.

2.2. Synthesis of the Ce_2S_3-CNT NCs

A simple wet-chemical method was used to synthesize Ce_2S_3-CNT NCs in an alkaline medium using cerium(III)chloride heptahydrate ($CoCl_3 \cdot 7H_2O$), sodium sulphide ($Na_2S \cdot 9H_2O$), and CNT. In the synthesis process, 50.0 mL of $CeCl_3$ solution (0.1 M) and 50.0 mL of Na_2S solution (0.1 M) were separately prepared in deionized (DI) water. Then, 1.0 mg of CNT was added to 50.0 mL of cerium(III)chloride solution in a conical flask and heated up to 85 °C for 30 minutes under continuous stirring. Later, 50.0 mL of the Na_2S solution was added dropwise to the abovementioned mixture under constant stirring. After 6 hours of continuous stirring at 85.0 °C, the reaction mixture was cooled down to room temperature and yielded black precipitate of the Ce_2S_3-CNT NCs. The black precipitate was washed by DI water and alcohol to remove any organic or inorganic impurities present and dried at room temperature. Then, the collected

Open Access Article. Published on 06 March 2017. Downloaded on 10/23/2025 5:22:54 PM.
This article is licensed under a Creative Commons Attribution 3.0 Unported Licence.

black powdered sample was dried at 65.0 °C using an oven for 6 h and finally the as-grown Ce_2S_3-CNT NCs were obtained.

The reaction scheme of Ce_2S_3-CNT NCs formation first depends on the slow release of Ce^{3+} and S^{2-} ions within the solution and second on the precipitation of these ions as Ce_2S_3 in and around the CNT. Formation of Ce_2S_3 depends on the fact that the ionic product of Ce^{3+} and S^{2-} ions is greater than the solubility product of Ce_2S_3. Ce^{3+} and S^{2-} ions are provided by the hydrolysis reactions of $CeCl_3$ and Na_2S, respectively. The proposed mechanism may be described as follows:

$CeCl_3$ gets ionized in water (eqn (i)) and dispersed in and around the CNT. Na_2S also gets ionized (eqn (ii)) and S^{2-} ions will also diffuse into the solution.

$$CeCl_3 \rightarrow Ce^{3+}{}_{(aq)} + 3Cl^{-}{}_{(aq)} \quad \text{(i)}$$

$$Na_2S \rightarrow 2Na^{+}{}_{(aq)} + S^{2-}{}_{(aq)} \quad \text{(ii)}$$

Effective collisions between Ce^{3+} and S^{2-} ions cause nucleation followed by aggregation and finally the formation of Ce_2S_3-CNT NCs in the presence of dispersed CNTs (eqn (iii)).

$$CNT_{(disp)} + 2Ce^{3+}{}_{(aq)} + 3S^{2-}{}_{(aq)} \rightarrow Ce_2S_3\text{-}CNT_{(s)}\downarrow \quad \text{(iii)}$$

The overall reaction can be written as follows (eqn (iv)):

$$2CeCl_{3(aq)} + 3Na_2S_{(aq)} + CNT_{(disp)} \rightarrow Ce_2S_3\text{-}CNT_{(s)}\downarrow + 6Na^{+}{}_{(aq)} + 6Cl^{-}{}_{(aq)} \quad \text{(iv)}$$

Finally, the as-grown Ce_2S_3-CNT NCs were washed by DI water and alcohol to remove any impurities present and dried at 65.0 °C using an oven. As-obtained Ce_2S_3-CNT NCs were characterized in detail for crystallinity, morphology, structural, electrochemical properties *etc.* and later used as a fabricating material on the GCE for the UA sensor in the simple *I–V* technique. In the Ce_2S_3-CNT NCs growth mechanism, at the beginning, growth of the Ce_2S_3 nucleus occurs by itself with mutual aggregation. As described by the Ostwald ripening method, later, nanocrystals re-aggregate to form combined γ-Ce_2S_3 nanocrystals.[33–36] In the presence of dispersed CNTs, γ-Ce_2S_3 nanocrystals crystallize and re-aggregate with one another and are deposited in and around CNT using van der Waals forces, which result in the porous morphology of the Ce_2S_3-CNT NCs, which is presented in Scheme 1.

2.3. Fabrication of GCE using Ce_2S_3-CNT NCs and detection of UA

Fabrication of GCE was carried out by the as-grown Ce_2S_3-CNT NCs using 5% ethanolic Nafion solution as the conducting binder. It was then heated in an oven at 65 °C for 2 h to obtain a dry film on GCE. In the electrochemical cell, a working electrode (WE) was made of the Ce_2S_3-CNT NC-coated GCE, whereas the counter electrode was made by a platinum (Pt) wire and aqueous UA in the buffer solution was the electrolyte. To use as target analytes, aqueous UA solution (0.1 M) was diluted to different concentrations (from 1.0 mM to 0.01 nM) using deionized water. All *I–V* measurements were carried out in 5.0 mL of phosphate buffer solution (PBS; 0.1 M; pH 7.0). From the slope of the current *vs.* voltage plot, the sensitivity of the proposed UA sensor was estimated.[37] Using an electrometer, *I–V* method was applied to UA solutions with Ce_2S_3-CNT NCs/GCE as the WE. Real samples were obtained from the medical center (KAU medical center). Initially, the rabbit serum was isolated from the blood. After dilution in PBS buffer, real serum and urine samples were analyzed *via* the fabricated Ce_2S_3-CNT NCs/GCE sensor using the *I–V* method under ambient conditions.

3. Results and discussion

3.1. Optical and structural evaluation

We analyzed the UV/vis spectrum (300–600 nm) of the as-grown Ce_2S_3-CNT NCs to obtain the band-gap energy (E_{bg}) of Ce_2S_3-CNT NCs. The broad peak at 493 nm was attributed to the characteristic peak of the Ce_2S_3, which is shown in Fig. 1(a). Using the UV/vis spectral data in the Tauc's equation, the E_{bg} for the Ce_2S_3-CNT NCs was calculated.[38–40] Tauc's equation (eqn (v)) can be represented as

$$\alpha h\nu = A(h\nu - E_{bg})^n \quad \text{(v)}$$

where $n = 1/2$ or 2 for a direct or indirect electronic transition, respectively. From the $(\alpha h\nu)^2$ *vs.* $(h\nu)$ plot (Fig. 1(b)), the E_{bg} for the as-grown Ce_2S_3-CNT NCs was estimated as ~2.31 eV, which is consistent with those of the previously reported Ce_2S_3-CNT NCs.

The FTIR spectrum of the as-grown Ce_2S_3-CNT NCs is shown in Fig. 1(c). Broad peaks at 3105 and 1475 cm^{-1} are due to the stretching and bending mode of vibration of water, respectively.[41] The stretching vibration of Ce_2S_3 gives a peak at 579 cm^{-1}. Peaks at 1159 and 980 cm^{-1} can be attributed to C–O single bond vibrations. The peak at 1730 cm^{-1} might be due to C=O. The C=S and C–S vibrational peaks occur at 1032 cm^{-1} and 627 cm^{-1}, respectively.[42]

The XRD pattern, as shown in Fig. 1(d), matched JCPDS # 50-0851 for the γ-Ce_2S_3 orthorhombic phase.[23] Peaks at 25.8° and 42.7° indicate the presence of CNT.[43–47] The more intense (211) peak at 23.2° implies that the (211) plane of the orthorhombic structure is slanted towards the experimental system. Overall, the whole XRD spectrum resembled that of the orthorhombic phase structure of γ-Ce_2S_3.

3.2. Morphological and elemental evaluation

The morphology and structure of the Ce_2S_3-CNT NCs were investigated by FESEM. Typical morphological information of the as-grown Ce_2S_3-CNT NCs is presented in Fig. 2(a)–(d). As-grown Ce_2S_3-CNT NCs exhibit interconnected networks of carbon nanotubes and Ce_2S_3 nanoparticles are adsorbed onto the CNT (white spots). This exceptional structure with self-assembled orthorhombic Ce_2S_3 nanoparticles provides a large surface area and increases the electron transport.

The chemical compositions were determined by the EDS analysis (Fig. 2(e) and (f)) of the as-grown Ce_2S_3-CNT NCs, which confirmed the presence of C, S, and Ce. Composition (wt%) of

Open Access Article. Published on 06 March 2017. Downloaded on 10/23/2025 5:22:54 PM.
This article is licensed under a Creative Commons Attribution 3.0 Unported Licence.

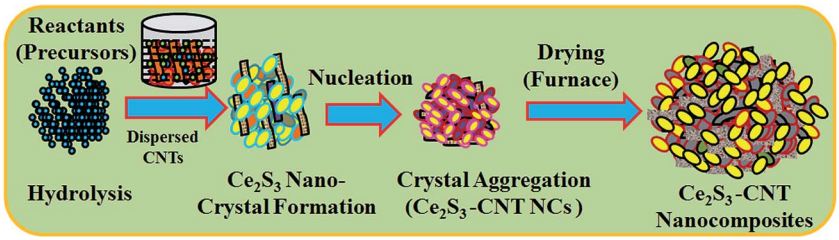

Scheme 1 Probable mechanism of Ce_2S_3-CNT nanocomposites synthesis *via* the wet chemical process.

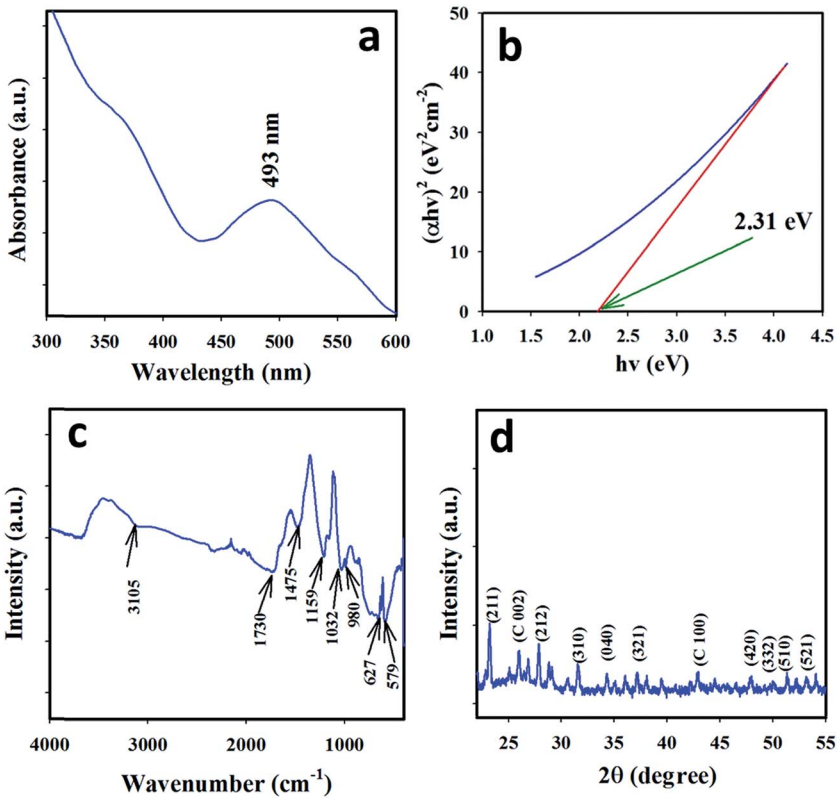

Fig. 1 Optical and structural evaluation: (a) UV/vis spectrum, (b) Tauc's plot for the E_{bg}, (c) FTIR spectrum, and (d) XRD spectrum of the as-grown Ce_2S_3-CNT NCs.

carbon, sulphur, and cerium in the as-grown Ce_2S_3-CNT NCs was 84.20%, 15.57%, and 0.23%, respectively. The absence of any other extra peak(s) (Fig. 2(f)) confirms the purity of the Ce_2S_3-CNT NCs.

3.3. Evaluation of binding energy

XPS was used for further investigation of the purity and nanostructure of the Ce_2S_3-CNT NCs. From the full scan spectrum (Fig. 3(a)), it can be deduced that the surface of the Ce_2S_3-CNT NCs consisted of cerium, sulfur, carbon, and oxygen atoms. Oxygen atoms present in the Ce_2S_3-CNT NCs may attach to carbon atoms by a carbon–oxygen single or double covalent bond or as C=O.[48] Obtained binding energy values of C1s and O1s of the as-grown Ce_2S_3-CNTNCs are 284.9 eV and 532.4 eV, respectively (Fig. 3(b) and (c)), which are very close to the reported values.[49] The Ce3d spectra consist of three well-resolved peaks (Fig. 3(d)) located at 933.6, 923.4, and 918.7 eV, corresponding to $Ce3d_{5/2}$, $Ce3d_{3/2}$, and $Ce3d_{1/2}$, respectively, which are also in good agreement with the binding energy of cerium in Ce_2S_3. As shown in Fig. 3(e), the two photoelectron signals at 164.2 and 169.4 eV can be attributed to $S2p_{3/2}$ and $S2p_{1/2}$, respectively, and the photoelectron signals at 228.4 eV, as shown in Fig. 3(f), can be attributed to S2s.[50] Main peaks in the XPS spectra (Fig. 3(a)–(f)) are consistent with those of previously reported Ce_2S_3.

4. Applications

4.1. Detection of UA using the Ce_2S_3-CNT NCs/GCE

UA in an aqueous solution was detected and the content was measured using the Ce_2S_3-CNT NC-fabricated GCE as the chemical sensor. Non-toxic nature, chemical stability, and

 This journal is © The Royal Society of Chemistry 2017

Open Access Article. Published on 06 March 2017. Downloaded on 10/23/2025 5:22:54 PM.
This article is licensed under a Creative Commons Attribution 3.0 Unported Licence.

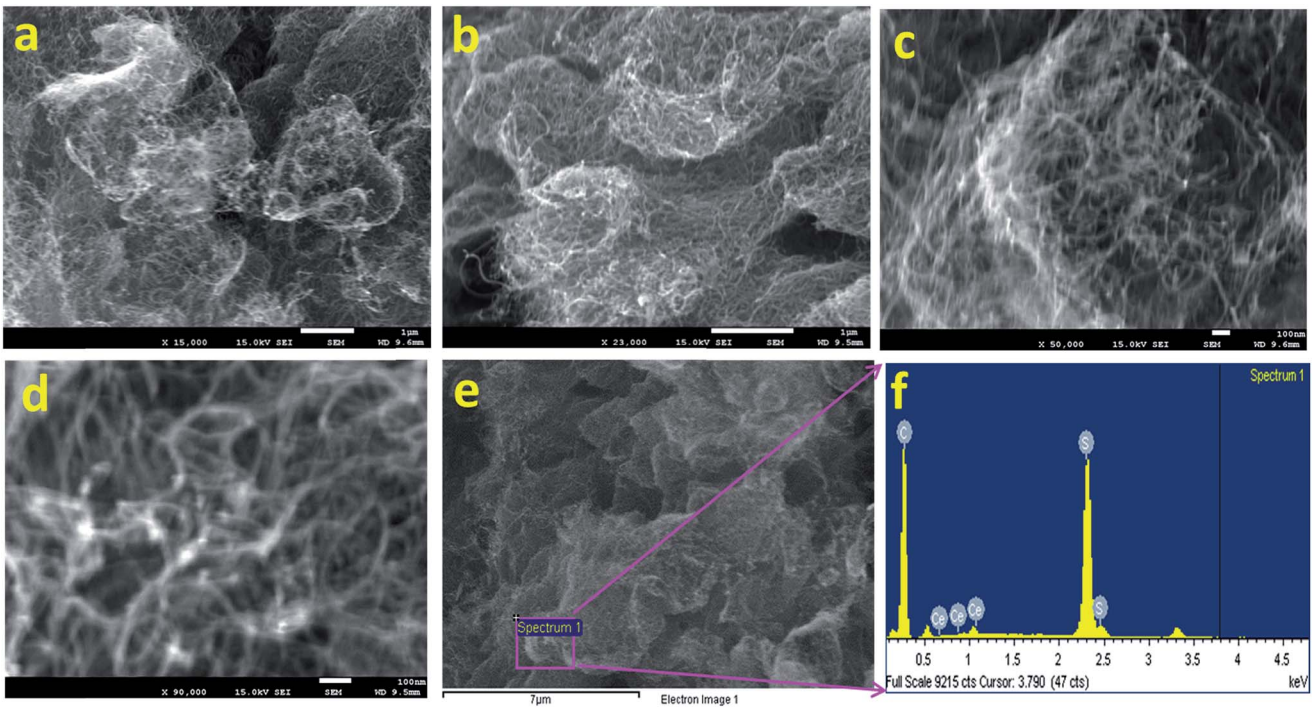

Fig. 2 Morphological and elemental evaluation. (a–d) Low to high-resolution FE-SEM images and (e and f) EDS spectrum for the as-grown Ce_2S_3-CNT NCs.

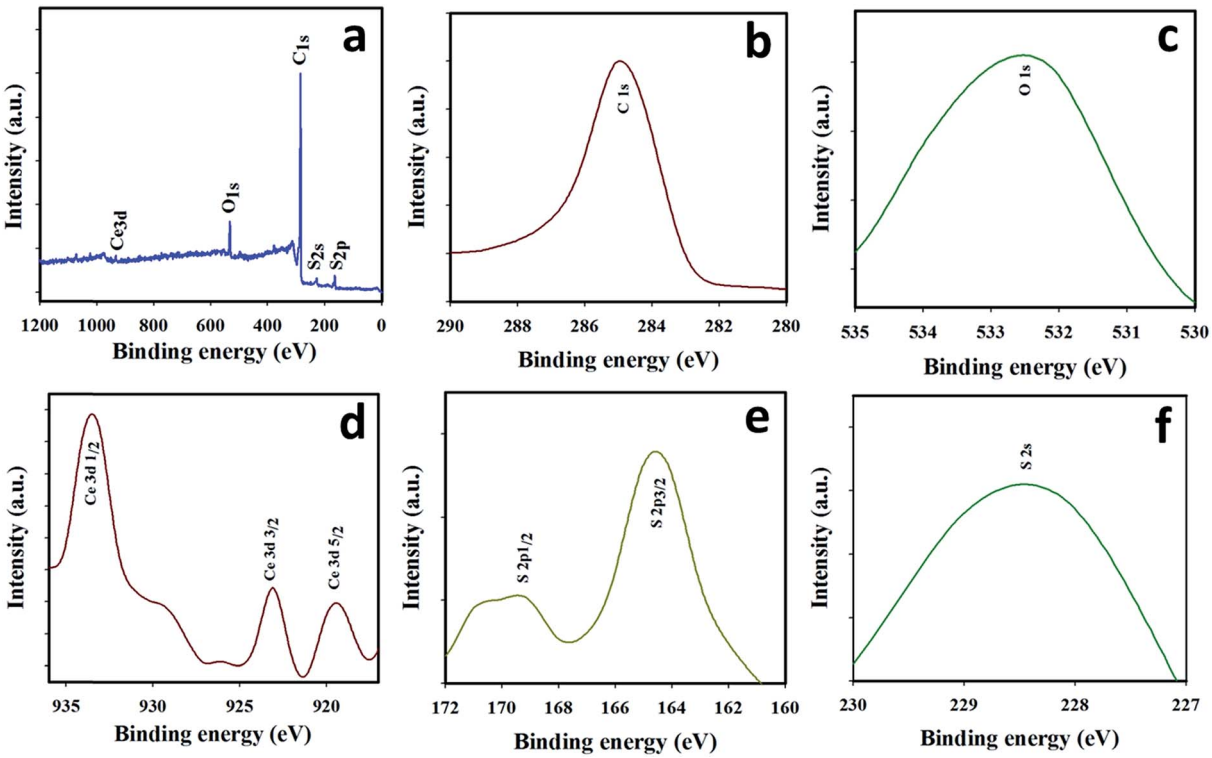

Fig. 3 Binding energy evaluation: XPS spectrum of (a) as-prepared Ce_2S_3-CNT NCs, (b) C1s, (c) O1s, (d) Ce3d, (e) S2p, and (f) S2s orbital acquired using MgKα_1 radiation.

electrochemical activity make the Ce_2S_3-CNT NCs one of the best sensing materials for UA. UA provided a remarkable response upon contact with the Ce_2S_3-CNT NCs in the *I–V* measurement. Fig. 4(a) shows the Ce_2S_3-CNT NCs/GCE electrode surface prepared in 5% ethanolic Nafion solution. The possible reduction scheme on the Ce_2S_3-CNT NCs/GCE is

Open Access Article. Published on 06 March 2017. Downloaded on 10/23/2025 5:22:54 PM.
This article is licensed under a Creative Commons Attribution 3.0 Unported Licence.

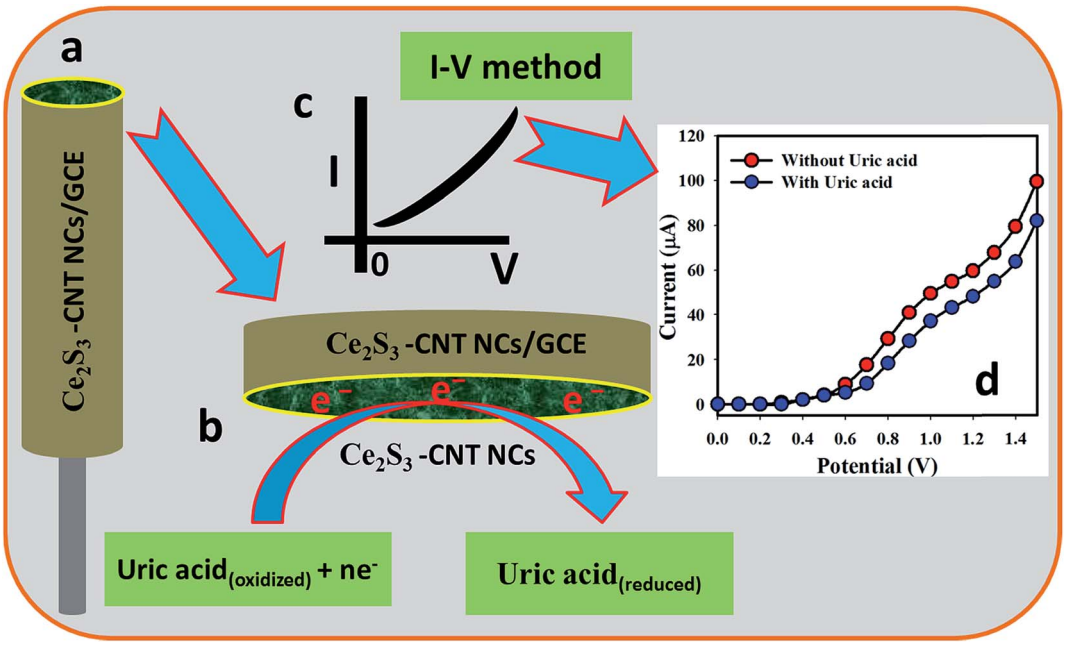

Fig. 4 Schematic for the (a) Ce_2S_3-CNT NC-coated rod-shaped round-GCE electrode with conducting Nafion (5% ethanol) coating binders, (b) proposed detection mechanism of UA, where UA is reduced by removing conducting electrons from the Ce_2S_3-CNT NCs/GCE electrodes, (c) theoretical outcome of *I–V* measurement, and (d) observed *I–V* response by the Ce_2S_3-CNT NCs/GCE with the delay time of 1.0 s.

generalized in Fig. 4(b), where UA gets reduced by gaining electrons from the conduction band of the Ce_2S_3-CNT NCs/GCE sensor surface during the *I–V* measurements, which decreases the current intensity with the increasing concentration at room temperature.[51–53] Fig. 4(c) shows the theoretical outcome, whereas Fig. 4(d) shows the practical *I–V* response with UA and without UA on the Ce_2S_3-CNT NCs/GCE working electrode at the delay time of 1.0 second in the electrometer, where a higher current response to the increasing voltage is clearly demonstrated.

4.2. Optimization and application of the UA biosensor

The electrochemical behavior of the Ce_2S_3-CNT NCs depends on the pH value. The pH dependence of the Ce_2S_3-CNT NCs was examined in PBS with different pH values (5.7 to 8.0), as shown in Fig. 5(a). These results demonstrate that the Ce_2S_3-CNT NCs show good electrochemical performance at various pH values. It can be well observed that on changing the pH value of the PBS, the electrocatalytic activity of the Ce_2S_3 CNT NCs changed, which is reflected by a variety of current responses. During the pH optimization using PBS (without using UA), the highest current response was obtained at pH 7.0. Therefore, pH 7.0 was kept constant throughout this study during the UA detection using the Ce_2S_3-CNT NCs/GCE assembly.

Current intensities in PBS (pH = 7.0) without UA for the bare GCE (blue dotted) and Ce_2S_3-CNT NCs/GCE (red-dotted) are given in Fig. 5(b). With the Ce_2S_3-CNT NCs/GCE, the current intensity is much higher as compared to that with the bare GCE for UA detection, which demonstrates the excellent electrochemical properties of the Ce_2S_3-CNT NCs. Fig. 5(c) demonstrates the current responses to seven biological analytes, where (1.0 μM; 25.0 μL) UA solution (red-dotted) in PBS (pH = 7.0) gave the best response with the Ce_2S_3-CNT NCs/GCE surface. Fig. 5(d) represents *I–V* responses of the Ce_2S_3-CNT NCs/GCE without UA (blue-dotted) and with UA (red-dotted; 1.0 μM; 25.0 μL) in 5.0 mL of PBS solution. In the presence of UA in PBS, a noticeable decrease in the current response implies the UA sensing ability of the developed Ce_2S_3-CNT NCs/GCE sensor. UA solution (25.0 μL) of different concentrations (from 0.1 nM to 0.1 M) was sequentially injected into 5.0 mL of PBS from the stock solutions and variations of surface current were investigated after every injection using the Ce_2S_3-CNT NCs/GCE as the WE, which is given in Fig. 5(e). It clearly demonstrates that the current response gradually decreases with the increasing concentration of UA at room temperature for the Ce_2S_3-CNT NCs/GCE sensor. Aqueous solutions of UA (from 0.01 nM to 1.0 mM) were obtained to investigate the detection limit of the proposed sensor. Fig. 5(f) represents the magnification of the concentration variation plot (Fig. 5(e)) from +0.6 to +1.5 V.

The calibration plot current *vs.* concentration (at +0.8 V) in the full concentration range is given in Fig. 6(a). A very high sensitivity value (1.5822 μA nM^{-1} m^{-2}) was calculated from the calibration plot at +0.8 V. The LDR of the proposed sensor was obtained from 0.1 nM to 1.0 mM ($r^2 = 0.9972$) and the LOD was calculated as 60.0 ± 0.05 pM [3 × noise (N)/slope (S)]. Fig. 6(b) represents the repeatability of the *I–V* responses with the as-grown Ce_2S_3-CNT NC-coated GCE using 25.0 μL of 0.1 μM UA solutions with nine different working electrodes in Run 1 – Run 9 under identical conditions. Almost the same current response in nine repeated experiments confirmed the excellent repeatability of the sensor (RSD = 3.52%, $n = 9$). This small % RSD may be due to the mass variation of the coating materials Ce_2S_3-CNT NCs in the working electrodes. When the same working

Open Access Article. Published on 06 March 2017. Downloaded on 10/23/2025 5:22:54 PM.
This article is licensed under a Creative Commons Attribution 3.0 Unported Licence.

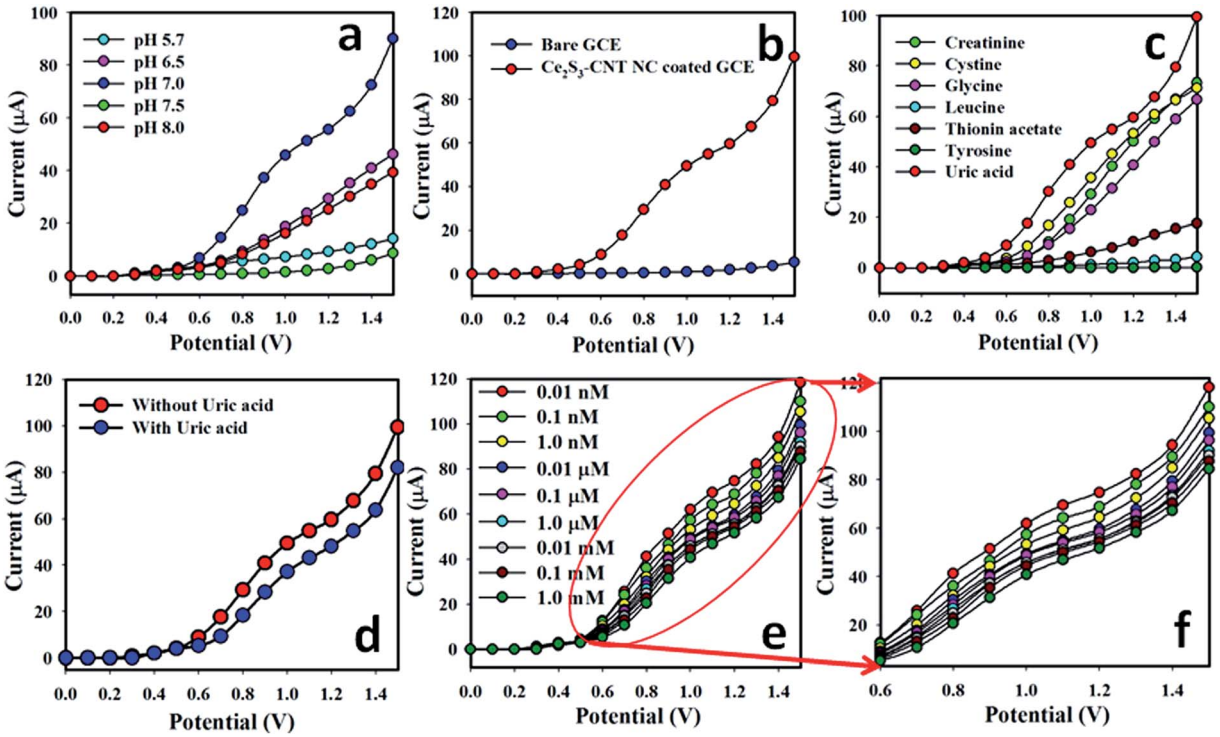

Fig. 5 *I–V* responses with a delay time of 1.0 s for (a) pH optimization of the Ce_2S_3-CNT NC-coated GCE, (b) bare and Ce_2S_3-CNT NC-coated GCE in PBS with UA, (c) selectivity study with various interferences (7 analytes) (d) in the absence and presence of UA (1.0 μM; 25.0 μL) in 5.0 mL of PBS solution, (e) current variations for different concentrations (from 0.01 nM to 1.0 mM) of aqueous UA solution in the full voltage range, and (f) magnified view of concentration variation (+0.6 to +1.5 V).

electrode was used in different solutions of the same concentration, even under identical conditions, current response slightly decreased. This is because after each run, the number of the active sites of the Ce_2S_3-CNT NCs slightly decreases.

4.3. Application to real samples

To confirm the validity of the *I–V* method, the Ce_2S_3-CNT NCs/GCE was used to quantify UA in two real aqueous UA solutions. For this purpose, we used the standard addition method to check the precision of the UA detection in aqueous samples (human urine and rabbit serum; Diluted 10 times in the buffer). A fixed amount (~25.0 μL) of real water sample was mixed and analyzed in PBS (5.0 mL) by the Ce_2S_3-CNT NCs/GCE working electrodes. Table 1 shows the results, which demonstrated that the amount of UA in the rabbit serum is higher than that in the urine sample. Based on the results, therefore, we can conclude that the *I–V* method is suitable, consistent, and appropriate in real sample analysis with the Ce_2S_3-CNT NCs/GCE system.

The resistance of the fabricated nanocomposites sensor decreases with the increasing electron communication, characteristics that are important features of the nanomaterial at RTP and *vice versa*.[54–58] During the reduction of UA, the number

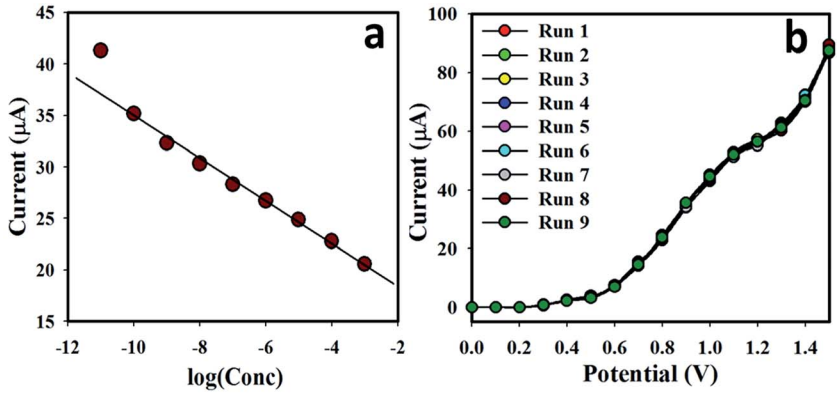

Fig. 6 (a) Calibration plot of Ce_2S_3-CNT NC-fabricated GCE surfaces. Potential range from 0.0 to +1.5 V and (b) repeatability using different WE (25.0 μL; 0.1 μM UA).

Open Access Article. Published on 06 March 2017. Downloaded on 10/23/2025 5:22:54 PM.
This article is licensed under a Creative Commons Attribution 3.0 Unported Licence.

Table 1 Quantification of uric acid in real samples

Real samples	Measured current (μA)	Respective concentration (nM)
Human urine (10 times diluted)	60.4	~1.50 ± 0.02
Rabbit serum (10 times diluted)	78.3	~2.12 ± 0.02

of electrons in the conduction band decreases and hence it increases the resistance of the Ce_2S_3-CNT NCs. Reduction of UA on the Ce_2S_3-CNT NCs surface is the main phenomenon involved in this proposed UA sensor. Due to its mesoporous structure, Ce_2S_3-CNT NCs have a large surface area that may be responsible for this sensitive reduction at room temperature. The rate of the UA reduction in Ce_2S_3-CNT NCs was higher than that of other analytes, even under identical conditions, as shown in Fig. 5(b). When UA is reduced on the Ce_2S_3-CNT NCs, it removes electrons from the conduction band of the nanocomposites, which increases the resistance of the coating material Ce_2S_3-CNT NCs.[59]

Current response in the *I–V* method during uric acid detection largely depends on the dimensions, morphology, and nanoporosity of the nanocomposites. When Ce_2S_3-CNT NCs surface is exposed to the oxidizing UA, a surface-mediated reduction reaction takes place. Removal of the conducting electrons from the Ce_2S_3-CNT NCs/GCE decreases the surface conductance of the electrode. This removal of electrons quickly decreases the conductance of the Ce_2S_3-CNT NCs coating. Massive deposition of the γ-Ce_2S_3 NPs on the CNT (white-spots in Fig. 2(a) and (b)) with porous morphology will increase the reducing power of the Ce_2S_3-CNT NCs. The Ce_2S_3-CNT NCs/GCE sensor requires approximately 10 s to achieve a constant current in the *I–V* measurements. It was practical to measure the response time, and the *I–t* plot is presented in the ESI (ESM, Ψ; Fig. S1†). This excellent sensitivity and high electrochemical performance of the Ce_2S_3-CNT NCs is due to the mesoporous surface that enhances the reduction of UA. The Ce_2S_3-CNT NCs/GCE sensor is more sensitive and has a lower detection limit than other sensors already reported for UA detection,[1–3,16–20,60] as given in Table 2. Having a large surface area, the Ce_2S_3-CNT NCs offered a positive nanoenvironment during the detection and quantification of UA. The Ce_2S_3-CNT NCs/GCE sensor has also shown better reliability and stability. Despite these developments, there are still numerous important apprehensions that must be investigated before the commercial production of this sensor.

5. Conclusions

In conclusion, we successfully fabricated GCE by the as-grown Ce_2S_3-CNT NCs with 5% ethanolic Nafion as the conducting coating binder for the first time to act as a selective chemical sensor for the detection of uric acid. Facile Ce_2S_3-CNT NCs were prepared by a wet-chemical method at low temperature, which is considered as the simplest, convenient, and economical method for the metal-sulphide nanocomposites preparation. The UA biological sensor was studied with Ce_2S_3-CNT NCs/Nafion/GCE by the simple *I–V* technique at room conditions. The analytical parameters were thoroughly investigated in terms of sensitivity, limit of detection, and storage ability as well as reproducibility. Significant research activities including synthesis, structural and optical characterization, and chemical-sensing application of the Ce_2S_3-CNT NCs towards the UA have been included in this study. Crystallinity, morphology, optical properties, band-gap, and binding energies were investigated by XRD, FESEM, FTIR, UV/vis spectroscopy, and XPS methods, respectively. The proposed Ce_2S_3-CNT NCs/GCE-based UA sensor exhibits the higher-sensitivity (1.5822 μA nM^{-1} m^{-2}) and very low detection limit (LOD = 60.0 ± 0.05 pM) with excellent linear response (r^2 = 0.9972) in a wide range of concentrations (from 0.1 nM to 1.0 mM) within a short response time. This noble approach is a well-organized and reliable technique of an effective biological sensor development for the detection of biological samples as well as biomolecules in the health care field.

Table 2 Analytical performance comparison of different detection methods for uric acid using various nanocomposites or nanomaterials on conventional electrodes

Electrode fabrication	Technique/method	Linear dynamic range (LDR)	Lower detection limit (LOD)	Sensitivity	pH	Ref.
Pristine graphene	CV + amperometry	6.00–1330 μM	4.82 μM	0.1029 μA μM^{-1}	7.0	1
Mesoporous NiO	CV	Up to 0.374 mM	0.005 μM	0.7562 μA μM^{-1} cm^{-2}	—	2
Gold nanocluster	Fluorescence	7.0×10^{-7} to 8.0×10^{-5} M	1.2×10^{-7} M	—	7.0	3
Au–Pt bimetallic nanoclusters	CV	0.125 μM to 8.28×10^{-2} M	4.07×10^{-2} μM	—	7.0	16
Polypyrrole films/Fe-substrate	CV	100–5000 μM	23.0 μM	0.0046 μA μM^{-1}	7.0	17
rGO/ZnS nanocomposites	DPV	1.0–500 μM	0.4 μM	—	7.0	18
Calixarene film	CV	0.4–40 μM	0.08 μM	—	—	19
Flexible graphene fibers	CV	10–26 μM	0.2 μM	—	7.0	20
Silver nanoprism	Colorimetry	1.0–40 μM	0.7 μM	—	—	60
Ce_2S_3/CNT NCs/Nafion/GCE	***I–V***	**0.1 nM to 1.0 mM**	**60.0 ± 0.05 pM**	**1.5822 μA nM^{-1} m^{-2}**	**7.0**	**This work**

 This journal is © The Royal Society of Chemistry 2017

Open Access Article. Published on 06 March 2017. Downloaded on 10/23/2025 5:22:54 PM.
This article is licensed under a Creative Commons Attribution 3.0 Unported Licence.

Acknowledgements

This project was funded by the Center of Excellence for Advanced Materials Research (CEAMR), King Abdulaziz University, Jeddah, under grant no. (CEAMR-SG-3-438).

References

1 S. Qi, B. Zhao, H. Tang and X. Jiang, Determination of ascorbic acid, dopamine, and uric acid by a novel electrochemical sensor based on pristine graphene, *Electrochim. Acta*, 2015, **161**, 395–402.

2 W. Huang, Y. Cao, Y. Chen, Y. Zhou and Q. Huang, 3-D periodic mesoporous nickel oxide for nonenzymatic uric acid sensors with improved sensitivity, *Appl. Surf. Sci.*, 2015, **359**, 221–226.

3 P. Xu, R. Li, Y. Tu and J. Yan, A gold nanocluster-based sensor for sensitive uric acid detection, *Talanta*, 2015, **144**, 704–709.

4 P. E. Erden and E. Kilic, A review of enzymatic uric acid biosensors based on amperometric detection, *Talanta*, 2013, **107**, 312–323.

5 L. Luo, F. Li, L. Zhu, Y. Ding, Z. Zhang, D. Deng and B. Lu, Simultaneous determination of epinephrine and uric acid at ordered mesoporous carbon modified glassy carbon electrode, *Anal. Methods*, 2012, **4**, 2417–2422.

6 K. Jindal, M. Tomar and V. Gupta, Nitrogen-doped zinc oxide thin films biosensor for determination of uric acid, *Analyst*, 2013, **138**, 4353–4362.

7 J. P. Dong, Y. Y. Hu, S. M. Zhu, J. Q. Xu and Y. J. Xu, A highly selective and sensitive dopamine and uric acid biosensor fabricated with functionalized ordered mesoporous carbon and hydrophobic ionic liquid, *Anal. Bioanal. Chem.*, 2010, **396**, 1755–1762.

8 W. R. Liu, *Modern Clinical Laboratory Diagnostics*, Chemical Industry Press, Beijing, 2009.

9 N. Maleki, A. Safavi, E. Farjami and F. Tajabadi, Palladium nanoparticle decorated carbon ionic liquid electrode for highly efficient electrocatalytic oxidation and determination of hydrazine, *Anal. Chim. Acta*, 2008, **611**, 151.

10 U. P. Azad and V. Ganesan, Determination of hydrazine by polyNi(II) complex modified electrodes with a wide linear calibration range, *Electrochim. Acta*, 2011, **56**, 5766.

11 F. Li, B. Zhang, S. Dong and E. Wang, A novel method of electrodepositing highly dispersed nano palladium particles on glassy carbon electrode, *Electrochim. Acta*, 1997, **42**, 2563.

12 J. Gu, X. Yang, C. Li and K. Kou, Synthesis of Cyanate Ester Microcapsules *via* Solvent Evaporation Technique and Its Application in Epoxy Resins as a Healing Agent, *Ind. Eng. Chem. Res.*, 2016, **55**, 10941–10946.

13 J. Gu, C. Liang, J. Dang, W. Dong and Q. Zhang, Ideal dielectric thermally conductive bismaleimide nanocomposites filled with polyhedral oligomeric silsesquioxane functionalized nanosized boron nitride, *RSC Adv.*, 2016, **6**, 35809–35814.

14 J. Gu, X. Meng, Y. Tang, Y. Li, Q. Zhuang and J. Kong, Hexagonal boron nitride/polymethyl–vinyl siloxane rubber dielectric thermally conductive composites with ideal thermal stabilities, *Composites, Part A*, 2017, **92**, 27–32.

15 J. Gu, X. Yang, Z. Lv, N. Li, C. Liang and Q. Zhang, Functionalized graphite nanoplatelets/epoxy resin nanocomposites with high thermal conductivity, *Int. J. Heat Mass Transfer*, 2016, **92**, 15–22.

16 H. Liu, J. Gao, W. Huang, K. Dai, G. Zheng, C. Liu, C. Shen, X. Yan, J. Guo and Z. Guo, Electrically conductive strain sensing polyurethane nanocomposites with synergistic carbon nanotubes and graphene bifillers, *Nanoscale*, 2016, **8**, 12977–12989.

17 H. Liu, W. Huang, X. Yang, K. Dai, G. Zheng, C. Liu, C. Shen, X. Yan, J. Guo and Z. Guo, Organic vapor sensing behaviors of conductive thermoplastic polyurethane–graphene nanocomposites, *J. Mater. Chem. C*, 2016, **4**, 4459–4469.

18 H. Liu, Y. Li, K. Dai, G. Zheng, C. Liu, C. Shen, X. Yan, J. Guo and Z. Guo, Electrically conductive thermoplastic elastomer nanocomposites at ultralow graphene loading levels for strain sensor applications, *J. Mater. Chem. C*, 2016, **4**, 157–166.

19 Y. Liu, P. She, J. Gong, W. Wu, S. Xu, J. Li, K. Zhao and A. Deng, A novel sensor based on electrodeposited Au–Pt bimetallic nano-clusters decorated on graphene oxide (GO)–electrochemically reduced GO for sensitive detection of dopamine and uric acid, *Sens. Actuators, B*, 2015, **221**, 1542–1553.

20 D. Oukil, L. Benhaddad, R. Aitout, L. Makhloufi, F. Pillier and B. Saidani, Electrochemical synthesis of polypyrrole films doped by ferrocyanide ions onto iron substrate: application in the electroanalytical determination of uric acid, *Sens. Actuators, B*, 2014, **204**, 203–210.

21 Y. J. Yang, One-pot synthesis of reduced graphene oxide/zinc sulfide nanocomposite at room temperature for simultaneous determination of ascorbic acid, dopamine and uric acid, *Sens. Actuators, B*, 2015, **221**, 750–759.

22 F. Wang, C. L. Chi, B. Yu and B. Ye, Simultaneous voltammetric determination of dopamine and uric acid based on Langmuir–Blodgett film of calixarene modified glassy carbon electrode, *Sens. Actuators, B*, 2015, **221**, 1586–1593.

23 W. Cai, J. Lai, T. Lai, H. Xie and J. Ye, Controlled functionalization of flexible graphene fibers for the simultaneous determination of ascorbic acid, dopamine and uric acid, *Sens. Actuators, B*, 2016, **224**, 225–232.

24 E. Ergün, S. Kart, D. K. Zeybek and B. Zeybek, Simultaneous electrochemical determination of ascorbic acid and uric acid using poly(glyoxal-bis(2-hydroxyanil)) modified glassy carbon electrode, *Sens. Actuators, B*, 2016, **224**, 55–64.

25 Y. Temerk and H. Ibrahim, A new sensor based on In doped CeO_2 nanoparticles modified glassy carbon paste electrode for sensitive determination of uric acid in biological fluids, *Sens. Actuators, B*, 2016, **224**, 868–877.

26 A. K. Bhakta, R. J. Mascarenhas, O. J. D'Souza, A. K. Satpati, S. Detriche, Z. Mekhalif and J. Dalhalle, Iron nanoparticles decorated multi-wall carbon nanotubes modified carbon

Open Access Article. Published on 06 March 2017. Downloaded on 10/23/2025 5:22:54 PM.
This article is licensed under a Creative Commons Attribution 3.0 Unported Licence.

paste electrode as an electrochemical sensor for the simultaneous determination of uric acid in the presence of ascorbic acid, dopamine and L-tyrosine, *Mater. Sci. Eng. C*, 2015, **57**, 328–337.

27 G. Zhang, P. He, W. Feng, S. Ding, J. Chen, L. Li, H. He, S. Zhang and F. Dong, Carbon nanohorns/poly(glycine) modified glassy carbon electrode: preparation, characterization and simultaneous electrochemical determination of uric acid, dopamine and ascorbic acid, *J. Electroanal. Chem.*, 2016, **760**, 24–31.

28 C. Alippi, A unique timely moment for embedding intelligence in applications, *CAAI Transactions on Intelligence Technology*, 2016, **1**, 1–3.

29 H. Jin, Q. Chen, Z. Chen, Y. Hu and J. Zhang, Multi-LeapMotion sensor based demonstration for robotic refine tabletop object manipulation task, *CAAI Transactions on Intelligence Technology*, 2016, **1**, 104–113.

30 J. C. Xing, Y. L. Zhu, Q. W. Zhou, X. D. Zheng and Q. J. Jiao, Fabrication and shape evolution of CoS_2 octahedrons for application in super capacitors, *Electrochim. Acta*, 2014, **136**, 550–556.

31 W. X. Mao, W. Zhang, Z. X. Chi, R. W. Lu, A. M. Cao and L. J. Wan, Core–shell structured Ce_2S_3@ZnO and its potential as a pigment, *J. Mater. Chem. A*, 2015, **3**, 2176.

32 S. Yu, D. Wang, Y. Liu, Z. Li, X. Zhang, X. Yang, Y. Wang, X. Wang and H. Su, Preparations and characterizations of γ-Ce_2S_3@SiO_2 pigments from precoated CeO_2 with improved thermal and acid stabilities, *RSC Adv.*, 2014, **4**, 23653.

33 M. M. Rahman, J. Ahmed and A. M. Asiri, Development of Creatine sensor based on antimony-doped tin oxide (ATO) nanoparticles, *Sens. Actuators, B*, 2017, **242**, 167–175.

34 M. M. Hussain, M. M. Rahman, A. M. Asiri and M. R. Awual, Non-enzymatic simultaneous detection of L-glutamic acid and uric acid using mesoporous Co_3O_4 nanosheets, *RSC Adv.*, 2016, **6**, 80511–80521.

35 M. M. Rahman, J. Ahmed, A. M. Asiri, I. A. Siddiquey and M. A. Hasnat, Development of ultra-sensitive hydrazine sensor based on facile CoS_2-CNT nanocomposites, *RSC Adv.*, 2016, **6**, 90470–90479.

36 M. M. Rahman, J. Ahmed, A. M. Asiri, M. A. Hasnat and I. A. Siddiquey, Development of 4-methoxyphenol chemical sensor based on NiS_2-CNT nanocomposites, *J. Taiwan Inst. Chem. Eng.*, 2016, **64**, 157–165.

37 C. Karuppiaha, S. Palanisamya, S. M. Chena, S. K. Ramarajb and P. Periakaruppan, A novel and sensitive amperometric hydrazine sensor based on gold nanoparticles decorated graphite nanosheets modified screen printed carbon electrode, *Electrochim. Acta*, 2014, **139**, 157–164.

38 M. M. Rahman, A. Jamal, S. B. Khan and M. Faisal, Highly Sensitive Ethanol Chemical Sensor Based on Ni-doped SnO_2 Nanostructure Materials, *Biosens. Bioelectron.*, 2011, **28**, 127–134.

39 X. Zhang, X. Yan, Q. He, H. Wei, J. Long, J. Guo, H. Gu, J. Yu, J. Liu, D. Ding, L. Sun, S. Wei and Z. Guo, Electrically Conductive Polypropylene Nanocomposites with Negative Permittivity at Low Carbon Nanotube Loading Levels, *ACS Appl. Mater. Interfaces*, 2015, 7(11), 6125–6138.

40 H. Wei, D. Ding, X. Yan, J. Guo, L. Shao, H. Chen, L. Sun, H. A. Colorado, S. Wei and Z. Guo, Tungsten Trioxide/Zinc Tungstate Bilayers: Electrochromic Behaviors, Energy Storage and Electron Transfer, *Electrochim. Acta*, 2014, **132**, 58–66.

41 R. Akbarzadeh, H. Dehghani and F. Behnoudnia, Sodium thiosulfate-assisted synthesis of NiS_2 nanostructure by using nickel(II)–Salen precursor: optical and magnetic properties, *Dalton Trans.*, 2014, **43**, 16745.

42 S. Pan, J. Zhu and X. Liu, Preparation, electrochemical properties, and adsorption kinetics of Ni_3S_2/graphene nanocomposites using alkyl dithiocarbonatio complexes of nickel(II) as single-source precursors, *New J. Chem.*, 2013, **37**, 654.

43 H. Liu, M. Dong, W. Huang, J. Gao, K. Dai, J. Guo, G. Zheng, C. Liu, C. Shen and Z. Guo, Lightweight conductive graphene/thermoplastic polyurethane foams with ultrahigh compressibility for piezoresistive sensing, *J. Mater. Chem. C*, 2017, **5**, 73–83.

44 M. M. Hussain, M. M. Rahman and A. M. Asiri, Sensitive L-leucine sensor based on a glassy carbon electrode modified with SrO nanorods, *Microchim. Acta*, 2016, **183**, 3265–3273.

45 H. Chen, T. Liu, J. Ren, H. He, Y. Cao, N. Wang and Z. Guo, Synergistic carbon nanotube aerogel – Pt nanocomposites toward enhanced energy conversion in dye-sensitized solar cells, *J. Mater. Chem. A*, 2016, **4**, 3238–3244.

46 M. M. Rahman, B. M. Abu-Zied, M. M. Hasan, A. M. Asiri and M. A. Hasnat, Fabrication of selective 4-amino phenol sensor based on H-ZSM-5 zeolites deposited silver electrodes, *RSC Adv.*, 2016, **6**, 48435–48444.

47 S. Guo, J. Liu, S. Qiu, Y. Wang, X. Yan, N. Wu, S. Wang and Z. Guo, Enhancing Electrochemical Performances of TiO_2 Porous Microspheres through Hybridizing with $FeTiO_3$ and Nanocarbon, *Electrochim. Acta*, 2016, **190**, 556–565.

48 E. Bi, H. Chen, X. Yang, W. Peng, M. Gratzel and L. Han, A quasi core–shell nitrogen-doped graphene/cobalt sulfide conductive catalyst for highly efficient dye-sensitized solar cells, *Energy Environ. Sci.*, 2014, **7**, 2637.

49 P. K. Chu and L. Li, Characterization of amorphous and nanocrystalline carbon films, *Mater. Chem. Phys.*, 2006, **96**, 253–277.

50 Z. Li, W. Li, H. Xue, W. Kang, X. Yang, M. Sun, Y. Tang and C. S. Lee, Facile fabrication and electrochemical properties of high-quality reduced graphene oxide/cobalt sulfide composite as anode material for lithium-ion batteries, *RSC Adv.*, 2014, **4**, 37180.

51 M. Zhang, B. Chen, H. Tang, G. Tang, C. Li, L. Chen, H. Zhang and Q. Zhang, Hydrothermal synthesis and tribological properties of FeS_2 (pyrite)/reduced graphene oxide heterojunction, *RSC Adv.*, 2015, **5**, 1417–1423.

52 M. M. Rahman, S. B. Khan, M. Faisal, A. M. Asiri and M. A. Tariq, Detection of aprepitant drug based on low-dimensional un-doped iron oxide nanoparticles prepared by solution method, *Electrochim. Acta*, 2012, **75**, 164–170.

Open Access Article. Published on 06 March 2017. Downloaded on 10/23/2025 5:22:54 PM.
This article is licensed under a Creative Commons Attribution 3.0 Unported Licence.

53 X. Chen, Z. Wang, X. Wang, J. Wan, J. Liu and Y. Qian, Single-Source Approach to Cubic FeS_2 Crystallites and Their Optical and Electrochemical Properties, *Inorg. Chem.*, 2005, **44**, 951–954.

54 M. M. Rahman and A. M. Asiri, Fabrication of highly sensitive ethanol sensor based on doped nanostructure materials using tiny chips, *RSC Adv.*, 2015, **5**, 63252–63263.

55 D. Y. Wang, M. Gong, H. L. Chou, C. J. Pan, H. A. Chen, Y. Wu, M. C. Lin, M. Guan, J. Yang, C. W. Chen, Y. L. Wang, B. J. Hwang, C. C. Chen and H. Dai, Highly Active and Stable Hybrid Catalyst of Cobalt-Doped FeS_2 Nanosheets–Carbon Nanotubes for Hydrogen Evolution Reaction, *J. Am. Chem. Soc.*, 2015, **137**, 1587–1592.

56 M. M. Rahman, A. Jamal, S. B. Khan, M. Faisal and A. M. Asiri, Highly Sensitive Methanol Chemical Sensor Based on Undoped Silver Oxide Nanoparticles Prepared by a Solution Method, *Microchim. Acta*, 2012, **178**, 99–106.

57 D. A. Rice, S. J. Hibble, M. J. Almond, K. A. H. Mohammad and S. P. Pearse, Novel low-temperature route to known (MnS and FeS_2) and new (CrS_3, MoS_4 and WS_5) transition-metal sulfides, *J. Mater. Chem.*, 1992, **2**, 895–896.

58 M. M. Rahman, S. B. Khan, A. M. Asiri and A. G. Al-Sehemi, Chemical sensor development based on polycrystalline gold electrode embedded low-dimensional Ag_2O nanoparticles, *Electrochim. Acta*, 2013, **112**, 422–430.

59 L. M. F. Dantas, A. P. dos Reis, S. M. C. N. Tanaka, J. H. Zagal, Y. Y. Chen and A. A. Tanaka, Electrocatalytic oxidation of hydrazine in alkaline media promoted by iron tetrapyridinoporphyrazine adsorbed on graphite surface, *J. Braz. Chem. Soc.*, 2008, **19**, 720–726.

60 D. Wu, H. F. Lu, H. Xie, J. Wu, C. M. Wang and Q. L. Zhang, Uricase-stimulated etching of silver nanoprisms for highly selective and sensitive colorimetric detection of uric acid in human serum, *Sens. Actuators, B*, 2015, **221**, 1433–1440.